Glutaconate CoA-transferase from *Acidaminococcus fermentans*: the crystal structure reveals homology with other CoA-transferases

Uwe Jacob[1]*, Matthias Mack[2], Tim Clausen[1], Robert Huber[1], Wolfgang Buckel[2] and Albrecht Messerschmidt[1]

Background: Coenzyme A-transferases are a family of enzymes with a diverse substrate specificity and subunit composition. Members of this group of enzymes are found in anaerobic fermenting bacteria, aerobic bacteria and in the mitochondria of humans and other mammals, but so far none have been crystallized. A defect in the human gene encoding succinyl-CoA: 3-oxoacid CoA-transferase causes a metabolic disease which leads to severe ketoacidosis, thus reflecting the importance of this family of enzymes. All CoA-transferases share a common mechanism in which the CoA moiety is transferred from a donor (e.g. acetyl CoA) to an acceptor, (*R*)-2-hydroxyglutarate, whereby acetate is formed. The transfer has been described by a ping-pong mechanism in which CoA is bound to the active-site residue of the enzyme as a covalent thiol ester intermediate. We describe here the crystal structure of glutaconate CoA-transferase (GCT) from the strictly anaerobic bacterium *Acidaminococcus fermentans*. This enzyme activates (*R*)-2-hydroxyglutarate to (*R*)-2-hydroxyglutaryl-CoA in the pathway of glutamate fermentation. We initiated this project to gain further insight into the function of this enzyme and the structural basis for the characteristics of CoA-transferases.

Results: The crystal structure of GCT was solved by multiple isomorphous replacement to 2.55 Å resolution. The enzyme is a heterooctamer and its overall arrangement of subunits can be regarded as an $(AB)_4$ tetramer obeying 222 symmetry. Both subunits A and B belong to the open α/β-protein class and can be described as a four-layered $\alpha/\alpha/\beta/\alpha$ type with a novel composition and connectivity of the secondary structure elements. The core of subunit A consists of seven α/β repeats resulting in an all parallel central β sheet, against which helices pack from both sides. In contrast, the centre of subunit B is formed by a ninefold mixed β sheet. In both subunits the helical C terminus is folded back onto the N-terminal domain to form the third layer of helices.

Conclusions: The active site of GCT is located at the interface of subunits A and B and is formed by loops of both subunits. The funnel-shaped opening to the active site has a depth and diameter of about 20 Å with the catalytic residue, Glu54 of subunit B, at the bottom. The active-site glutamate residue is stabilized by hydrogen bonds. Despite very low amino acid sequence similarity, subunits A and B reveal a similar overall fold. Large parts of their structures can be spatially superimposed, suggesting that both subunits have evolved from a common ancestor.

Addresses: [1]Max Planck Institut für Biochemie, Abteilung Strukturforschung, Am Klopferspitz 18a, D-82152 Martinsried, Germany and [2]Laboratorium für Mikrobiologie des Fachbereichs Biologie der Phillips Universität Marburg, D-35032, Germany.

*Corresponding author.
E-mail: ujacob@libelle.biochem.mpg.de

Key words: coenzyme A, crystal structure, fermentation, glutamate, transferase

Received: 6 November 1996
Revisions requested: 13 December 1996
Revisions received: 2 January 1997
Accepted: 15 January 1997

Electronic identifier: 0969-2126-005-00415

Structure 15 March 1997, 5:415–426

Introduction

The characterization of acyl-CoA thiol esters by Lynen and co-workers [1] highlighted two distinct properties of this biologically important class of compounds, namely the electrophilic nature of the ketone-like carbonyl carbon and the acidity of the hydrogens at the α carbon. These properties are exploited in numerous enzyme catalyzed conversions, such as CoA and acyl transfers as well as ester and Claisen condensations (e.g. in citrate synthesis). CoA-transferases catalyze four subsequent nucleophilic attacks on carbonyl carbons, which result in the reversible transfer of the CoA moiety from an acyl-CoA to a carbonic acid (Fig. 1). Glutaconate CoA-transferase (GCT) from the strictly anaerobic bacterium *Acidaminococcus fermentans*, which thrives in the intestine of animals and humans [2], is involved in the fermentation pathway of glutamate [3]. GCT catalyzes the transfer of the CoA moiety from acetyl CoA to (*R*)-2-hydroxyglutarate and related compounds like glutaconate, from which the name of the enzyme derives. As the 'energy-rich' thiol ester bond is conserved in this reaction,

Figure 1

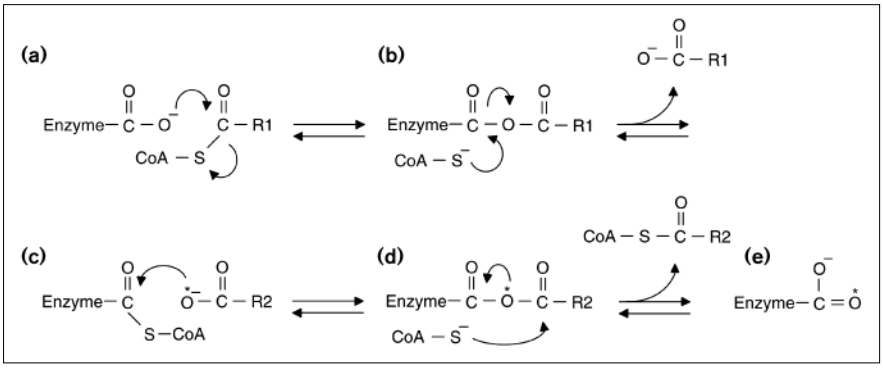

The reaction mechanism of CoA-transferases. Coenzyme A (CoA–SH) is transferred from one substrate (R1–CO–S–CoA) to the second substrate (R2–COO^-). A carboxy group of a certain glutamate residue of the enzyme (enzyme–COO^-) is directly involved in catalysis and binds CoA transiently as a thiol ester. Details of the reaction mechanism are given in the text. The asterisk denotes the oxygen atom that is transferred to the enzyme.

this mode of carboxylate activation is preferred by anaerobic fermentative bacteria which have to cope with low ATP yields [2,4–11]. CoA-transferases are also found in aerobic bacteria [12] (MS Shanley, A Harrison and LN Ornston, (1991) GenBank entries: pir A44570 and B44570) and in the related mitochondria of man and animals. Here, the succinyl-CoA:3-oxoacid CoA-transferase catalyzes the activation of D-3-hydroxybutyrate and acetoacetate, which is the rate-limiting step in ketone body metabolism [13–16]. CoA-transferases are a heterogeneous family of enzymes with differing substrate specificities, that appear in a variety of non-cooperative oligomerization states. These states range from monomers (A), in the case of oxalate formyl CoA-transferase from *Oxalobacter formigenes* (M_w = 44 kDa) [11], to heterooctamers $(AB)_4$, in the case of GCT (M_w = 260 kDa) [2]. It has been shown that the A chain of the pig heart 3-oxoacid CoA-transferase (subunit composition $(A)_2$) arose from a gene fusion of bacterial A and B chains.

GCT was purified and crystallized from cell-free extracts from *A. fermentans*. The two genes coding for the A (M_w = 35 kDa) and B (M_w = 29 kDa) subunits have been cloned and overexpressed in *Escherichia coli* [3]. There is no immediate apparent sequence similarity to other CoA-transferases of known primary structures. The sequences of the other CoA-transferases are more closely related to each other, probably due to their common specificity for 3-oxoacid substrates [12,17,18] (GenBank entries: pir A44570 and B44570).

Despite these differences all CoA-transferases follow a common reaction mechanism. Exceptions to this are the homodimeric α subunits of citrate and (*S*)-citramalate lyases, in which a direct transfer of the CoAS moiety from acetyl CoA to citrate or citramalate was observed [19–22]. Therefore, these later two enzyme complexes are not considered further in this work.

The general reaction mechanism of CoA-transferases was elucidated by Jencks and co-workers studying pig heart 3-oxoacid CoA-transferase and is depicted in Figure 1 [23]. They showed that the CoAS moiety was not transferred directly to the carboxylate substrate. Instead a specific glutamate residue at the active site of the enzyme (a) forms a covalent thiol ester intermediate (c). Hence, the reaction follows a ping-pong mechanism in which the first product, carboxylate-1 (b) is released before the second substrate, carboxylate-2 (d), enters the catalytic pathway. The two consecutive CoAS transfers require two mixed anhydrides (b,d) as additional intermediates, these are protected from hydrolysis by the apparently hydrophobic environment of the active site. Evidence for the formation of such anhydride intermediates has been obtained from model reactions [19]. Thus, the whole catalytic cycle consists of four subsequent nucleophilic attacks on electrophilic carbonyl groups, alternately by carboxylate and thiol anions, whereby the carbonyl oxygens acquire transient net negative charges. GCT follows the general reaction mechanism and the essential active-site residue was identified by chemical methods and site-directed mutagenesis [2,3,24,25] to be Glu54 on subunit B.

We present here the spatial structure of GCT, solved by multiple isomorphous replacement (MIR) to 2.55 Å resolution. The structure shows the homology of the subunits, their interplay to form the active site and the implications on the mechanism of this enzyme. Suggestions on the relation to the other CoA-transferase are made.

Results and discussion

Structure analysis

The octameric structure of GCT can be regarded as a tetramer of heterodimers associated in *222* symmetry. The asymmetric unit contains two dimers termed A1B1 and A2B2 that are related by noncrystallographic symmetry (ncs), a rotation of 179.9°. The model includes all amino acid residues except for the leading methionines and the N- and C-terminal residues Asp319A, Lys320A, Ala2B and Thr263B–Lys266B that are disordered. The ncs-related A2B2 dimer contains the same residue range, but the electron density for the sidechain of Glu202B is missing.

Table 1

Refinement statistics.

Resolution range (Å)	7.0–2.5
No. unique reflections ($F > 0\sigma$ (F))	37 201
Completeness (%)	
overall (7.0–2.55 Å)	83
2.55–2.64 Å shell	32
R factor	0.19
R_{free}*	0.27
No. heavy atoms per asymmetric unit	
protein	8994
solvent	438
Cu^{2+}	1
Rms deviation from ideal geometry	
bond length (Å)	0.01
bond angle (°)	1.8
Average B factors (Å^2)	
protein mainchain	23
protein sidechain	24
solvent	34
Ca^{2+}	39
Rms deviation of bonded B factors (Å^2)	2.8

*The R_{free} was derived by repeating the final refinement using 5% of the reflections as a reference set. Model bias was reduced by including a 1000K simulated annealing step.

Beside 438 water molecules the model contains one copper ion derived from the crystallization buffer that is coordinated to two different His16A residues of adjacent asymmetric units and was indispensable for crystallization. This copper ion, as well as a water molecule (Wat438), are located in special positions and are consequently shared by two asymmetric units.

The refinement statistics are summarized in Table 1. The mean coordinate error is approximately 0.31 Å, as calculated according to Luzzati [26]. The root mean square (rms) deviation from ideal bond length and bond angle values of the standard geometry [27] are 0.010 Å and 1.8°, respectively.

The models of the ncs-related subunits A1B1 and A2B2 are virtually identical as can be seen from the low rms difference between their α carbon positions (0.29 Å for subunits A1/A2 and 0.36 Å for B1/B2 [28]). Appreciable differences between the ncs-related subunits are of two kinds: either one of the ncs-mates is involved in a crystal contact or the variable residues are located in the flexible terminal regions and are associated with high B factors. Nevertheless, no individual distances between related Cα carbons are larger than 1.2 Å.

The mainchain torsion angles of all amino acid residues are located in the allowed regions of the Ramachandran plot except for Thr27A and Ile171B, where the averaged ϕ/ψ values for the ncs-related molecules are -103/37 and –89/59, respectively [29]. The sterical conformation of these two residues is reliable and justified by well defined electron density in both ncs views of the molecule. Thr27A is located in a turn (of type II′, [30]) contributing to the active site and defined by hydrogen bonds to Ser78A and Ala53A. Ile171B is also found within a turn (type IV) adjacent to the bulky sidechain of Trp170B. Its position is confirmed by low B factors as well as hydrogen bonds to Asn116B and a solvent molecule.

Overall structure of the monomers

Both subunits A and B of GCT from *A. fermentans* belong to the open α/β-protein family and can be described as four-layered α/α/β/α type. However, the topology of both subunits is novel and differs considerably from other members of the α/β-protein class including the nucleotide-binding domains (Fig. 2). The core of subunit A consists of a classical sevenfold α/β repeat leading to the central seven-stranded all parallel β sheet. The helices α1–α4 pack against one side of the central β sheet and helices α5, α7 and α8 pack against the other side. The large extension between helix α5 and strand β8 is folded into a small threefold antiparallel β sheet (β5–β7) and a short helix (α6). The predominantly helical C-terminal region of subunit A is composed of the helices α9–α12 that are packed against the N-terminal part thereby forming the third layer of helices. Pro247A is connected via a *cis* peptide bond within a class VIa turn to the preceding His246A. This turn terminates the central β sheet after β10 in subunit A and leads to the C-terminal third α helical layer.

The overall fold of subunit B is related to subunit A

The core of subunit B comprises six α/β repeats which are involved in the formation of the central nine-stranded mixed β sheet. In analogy to the four helices in subunit A, the single C-terminal helix α8 in subunit B packs against the N-terminal region and occupies the position of the third helical layer. Between the fourth and fifth α/β repeats a 25 amino acid residue extension is folded into a short two-stranded antiparallel β sheet, which protrudes from the protein core and interacts with subunit A. The first seven secondary structure motifs of subunit B resemble the structure of subunit A although the direction of β3 is reversed and, consequently, the corresponding α helix of the third α/β motif is missing. The two C-terminal antiparallel strands, β10 and β11, extend the number of strands in the central β sheet of subunit B to nine. Due to the lack of these strands in the central β sheet of subunit A, the β sheet in this subunit is all parallel seven-stranded.

Quaternary structure

GCT is composed of AB heterodimers which associate to form heterotetramers located within one asymmetric

Figure 2

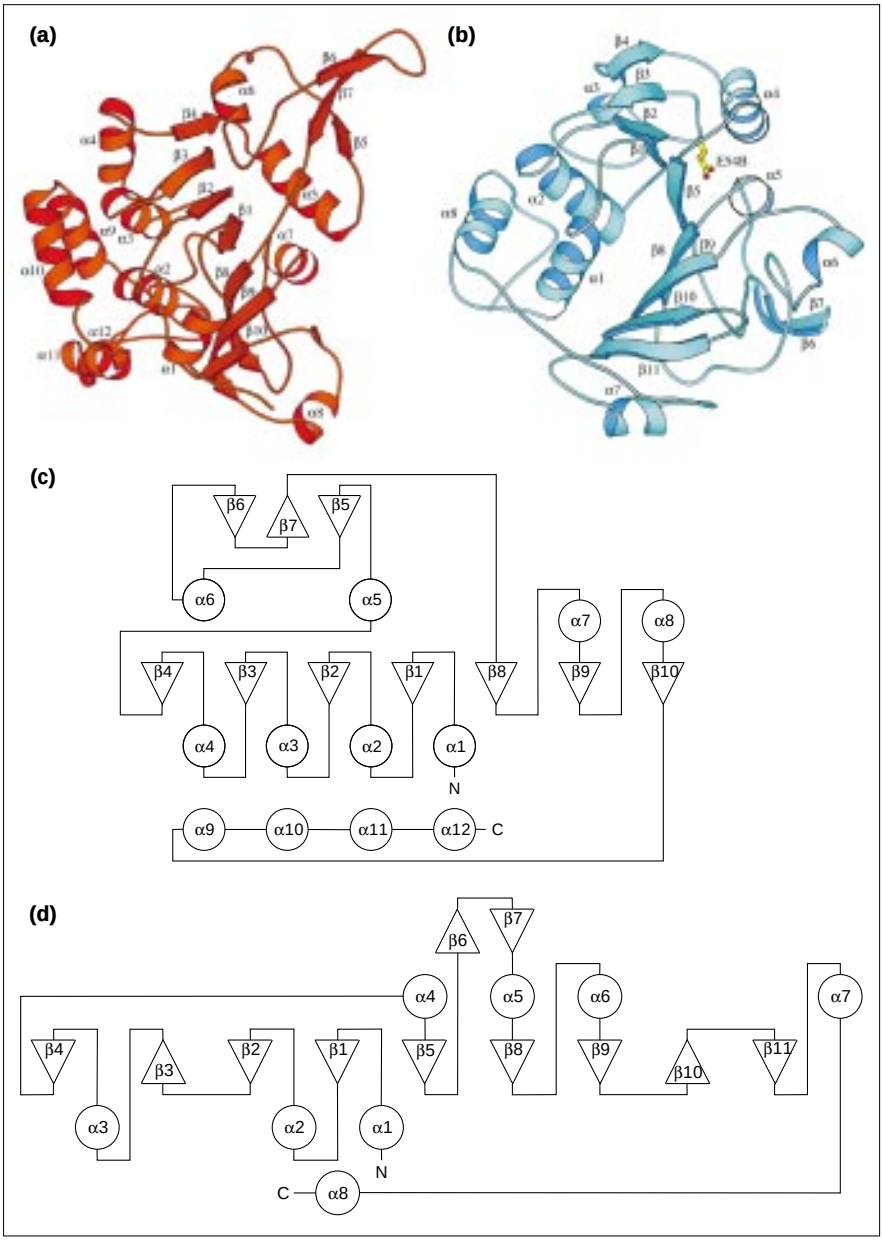

The fold of *A. fermentans* GCT. Ribbon representation of the secondary structure motifs of (a) subunit A (red) and (b) subunit B (blue). Secondary structure elements are numbered consecutively from the N terminus to the C terminus; α denotes helices and β denotes strands. The active-site residue, Glu54B, is labelled in subunit B and shown in ball-and-stick representation. (The figure was generated with MOLSCRIPT [43].) (c,d) Topographical diagrams of subunits A and B of GCT, respectively. Circles represent α helices and β strands are represented by triangles; the triangles point downwards if the corresponding strand runs from front to back in the view shown in parts (a) and (b) of this figure. The N and C termini are indicated and the numbering is consistent with parts (a) and (b).

unit. The functional enzyme is a heterooctamer of two heterotetramers.

The heterodimer is built by an edge to edge interaction of the two central β sheets of subunit A and B (Fig. 3). The contacts are mediated by loops at the C-terminal ends of the β strands of both subunits. Additional contacts are made by the protrusion of subunit B containing the strands β6 and β7; this region probably evolved just for this purpose.

The heterotetramer is formed by two AB heterodimers related by a twofold noncrystallographic axis (Fig. 4a). Rotation around this dyad relates subunit A1 to A2 and subunit B1 to B2, so that the contacts of subunits A1 and B1 are equivalent to the contacts of subunits A2 and B2. Therefore, two different contacts are encountered that contribute to the heterotetramer formation: subunit A1 interacts with its ncs mate A2 and subunit A1 interacts with B2 (the ncs mate of B1). The ncs-related subunits B1 and B2 do not interact with each other.

The A1–A2 contact is dominated by the extra three-stranded β sheet (strands β5 to β7) of subunit A that protrudes from the core. Analogous to the β6/β7 sheet in

Figure 3

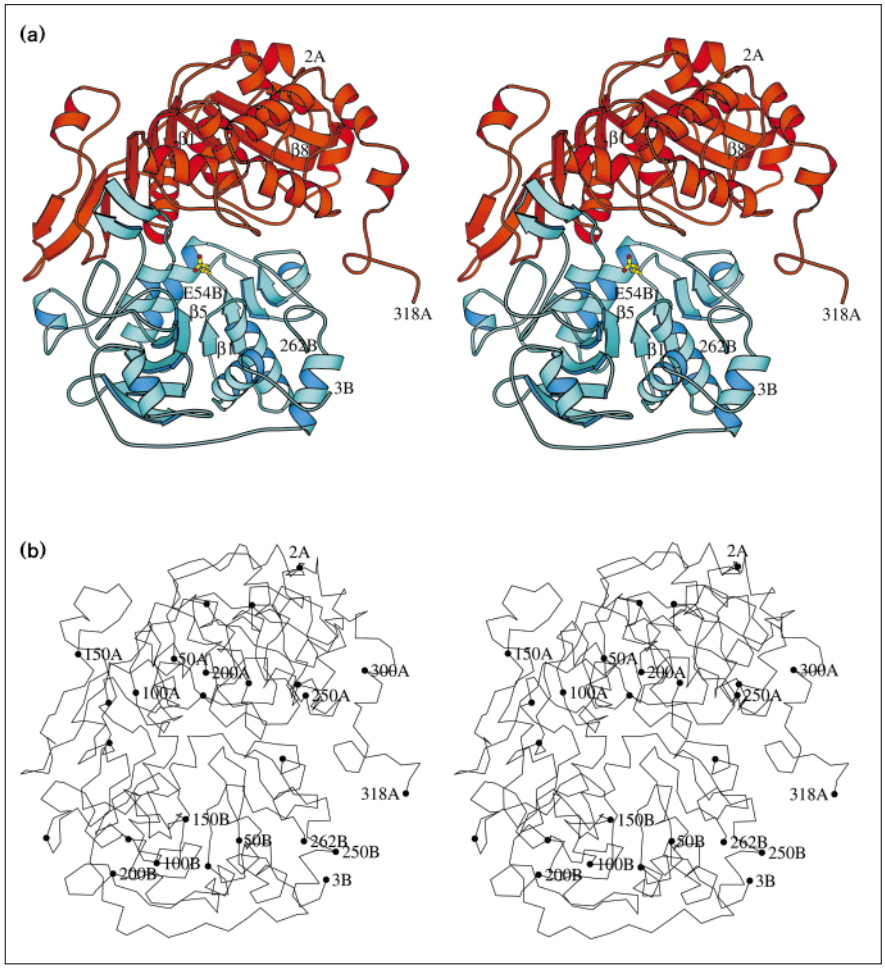

The close interaction of GCT subunits A and B in the formation of the active site. **(a)** Stereoscopic drawing of the interaction of GCT subunit A (red) and subunit B (blue). The N and C termini are marked together with the four strands which are referred to in the text; the active-site glutamate is shown in ball-and-stick representation. **(b)** Stereoscopic Cα trace of subunits A and B in the same orientation as depicted in (a). Every 25th residue is marked and every 50th labelled; the N and C termini are also labelled. (The figure was produced using the program MOLSCRIPT [43].)

subunit B, this extension is responsible for the structural integrity of the complex. The interface between A1 and B2 is built by β4 and α4 of subunit B2 packing against the α helical layer α5, α7 and α8 of A1. As a consequence, α4 of subunit B2 is involved in contacts to subunit A1 as well as to A2.

The octamer is composed of the two tetramers A1, B1, A2, B2 and A1*, B1*, A2*, B2* (Fig. 4b), which are related by a twofold crystallographic symmetry. As the ncs dyad intersects the crystallographic axis at an angle of 90° in the centre of this complex, the whole octamer follows a 222 symmetry. The interaction between subunit A1 and A1* is realized by the α helical C-terminal region of both subunits. Due to the symmetry relation an equivalent contact relates subunits A2 and A2*. In contrast all B-like subunits do not contribute to the stability of the octamer.

The buried surface within the heterodimer has an estimated value of 1847 Å^2, within the heterotetramer of 2560 Å^2 and within the octamer of 2147 Å^2 (as calculated with the CCP4 package [31]). Because the buried surface is related to the interaction energy of the involved subunits and the contact area of further crystal contacts except for the tetramer–tetramer contact is small, it can be proposed that the octamer observed in the crystals is equivalent to the functional enzyme complex found in solution. This is consistent with the observation that GCT elutes from a molecular sieve column as an octamer [2]. Based on the knowledge of the subunit arrangement it can be predicted that the deletion of the C terminus of subunit A will reduce the oligomeric state from octameric to tetrameric.

The active site

As can be predicted from a dimer of the open α/β-protein class, the active site of GCT is located at the interface of the two subunits where the carboxy ends of the parallel β strands face each other (Fig. 3) [32]. In comparison to other α/β structures, the opening of the active site is formed by the two adjacent loop regions in subunit B that connect the strands β1 and β5 to α helices on opposite

Figure 4

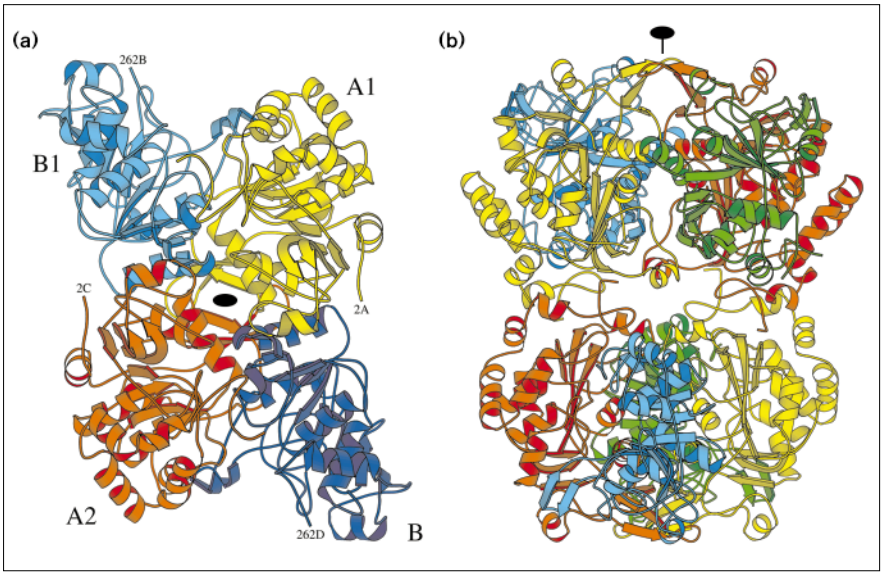

The quaternary structure of the GCT assembly. (a) Ribbon representation of the heterotetrameric assembly of GCT. The subunits are labelled: A1 (yellow), B1 (light blue), A2 (red) and B2 (dark blue). The view is chosen along the noncrystallographic symmetry dyad relating A1–B1 with A2–B2. (b) View of the complete GCT octamer, the orientation is tilted by 90° as compared to (a). The local twofold axis runs from the top to the bottom. (The figure was produced using the program MOLSCRIPT [43].)

sites of the β sheet. Additional regions of subunit B lining the active site are located in loops following β3 and β7, whereas the bottom of the site is sealed by residues of helix α4. Subunit A packs against this crevice, thereby closing it to a funnel-shaped opening. The regions of subunit A that contribute to the active site are, as in subunit B, the carboxy ends of the β strands β1 and β8, which are connected to helices on opposite sides of the central β sheet. Additional amino acids of subunit A that contribute to the active site are located on the loops following the strands β2, β3 and parts of helix α5.

Labelling experiments and mutational analysis, performed by Mack and Buckel [25], unambiguously demonstrated that Glu54B is the key residue that reacts with acetyl CoA in order to form the postulated stable intermediate. This residue is positioned at the bottom of the funnel, which is approximately 20 Å deep and 20 Å wide. The entrance of the active site is surrounded by positively charged residues, as shown in Figure 5. The distance between one pair of positive charges, Lys10B and Arg157B, is about 12 Å and this matches the distance between the negative charges of the phosphoryl groups in the adenine moiety of CoA (9 Å). The extended sidechains of the Lys10B and Arg157B are not flexible, as indicated by atomic B factors. Arg157B is held in its position by a salt bridge to Glu154B. Lys10B is involved in hydrogen bonding to the mainchain carbonyls of Phe258B and Gln260B, as well as in a hydrophobic interaction with Leu33B (Fig. 6).

The catalytic residue Glu54B is involved in hydrogen bonding to two residues, namely to the mainchain amide of Gly137B, which is conserved, and to the sidechain amide of Gln103A. As Glu54B is probably negatively charged at the pH of crystallization (pH = 5.5), this interaction mimics the stabilization of the postulated oxyanions of the tetrahedral transient intermediates (Fig. 1) [23].

CoA-binding experiments were carried out, but neither soaking of native crystals nor co-crystallization with acetyl CoA lead to interpretable difference density maps. However, density was observed connected to Glu54B, which would correspond to the proposed thiol ester intermediate upon reaction with acetyl CoA. This density faded away quickly while tracing the panthothenate unit of CoA, indicating that it is either flexible or that the intermediate species has low occupancy. It was not possible until now to circumvent these problems by adding excess acetyl CoA and deep freezing the crystals. Additional difference density was found in the vicinity of the positively charged amino acids Lys10B and Arg157B, which is thought to correspond to the phosphoryl groups of the CoA moiety.

As GCT belongs to the class of open α/β proteins and the CoA moiety contains a mono-nucleotide we inspected the GCT structure for a mononucleotide-binding motif, which is arranged in the so-called 'Rossmann fold'. This binding motif comprises a pair of two parallel β strands connected by an antiparallel α helix; the motif has a characteristic amino acid sequence of GXGXXGX(17–21 residues)D/E. Within the classical Rossman fold the first two glycine residues are located in the loop connecting the N-terminal β strand with the helix. The third glycine of the motif is located in the helix and the aspartate or glutamate residue is positioned at the C terminus of the second β strand and

Figure 5

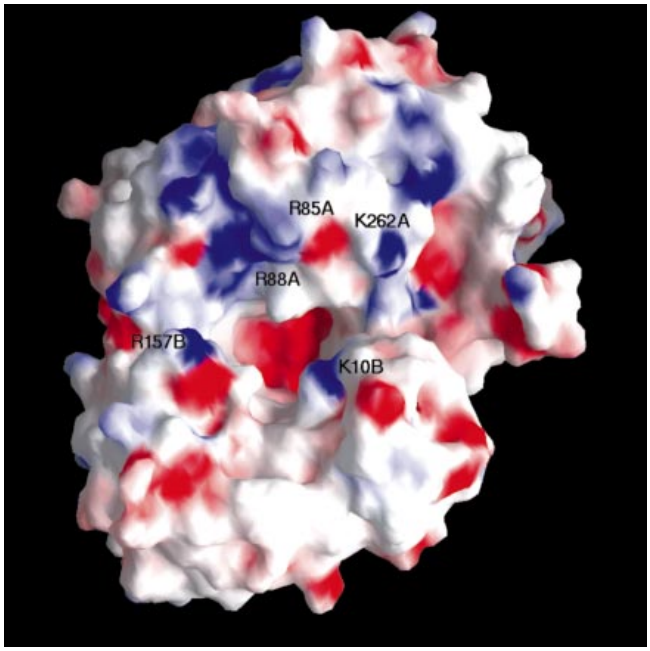

Surface potential map of the GCT dimer. Solid-surface representation of the GCT dimer as produced with GRASP [44], the colour-coding is according to the surface potential from negative (red) to positive (blue). The view is down the active-site funnel, at the interface of subunits A (upper part) and B (lower part). Positively charged residues around the active-site opening are labelled. The bottom of the active site is negatively charged (red) due to the presence of Glu54B (not labelled).

forms hydrogen bonds to the OH groups of the ribose of the bound nucleotide. The only possible candidate for a Rossmann fold in GCT is the β/α/β motif preceding the active-site residue, Glu54B. A spatial superposition of the mononucleotide-binding motif of liver alcohol dehydrogenase (LADH) (residues 194–224) onto the β/α/β motif of GCT (residues 24B–55B, including the active-site Glu54B) was done on an interactive graphical display. The most reasonable superposition is obtained when the two α helices are superimposed. This superposition shows that the amino acids at corresponding spatial positions are so different that the two β strands in GCT are moved away from the α helix in comparison to LADH. As a consequence the sidechain of Glu54B is about 4 Å away from the position of the sidechain of Asp223, the spatially equivalent residue in LADH. Glu54B as the active-site residue in GCT binds to the CoA moiety and can therefore not participate in the binding of a nucleotide.

It is intriguing that in GCT a similar nucleotide-binding motif can be found but here the important aspartate/glutamate function has been used as an active-site residue. Additionally, this analysis shows that the mononucleotide of CoA will most probably bind in another way, as in the classical Rossmann fold.

A hypothesis for the catalytic action of GCT

Negatively charged substrates, such as glutaconate or the phosphoryl groups of the nucleotide moiety of CoA, are attracted by the positive charges at the entrance of the active site. CoA binds through its phosphoryl groups to Lys10B and Arg157B, and the aromatic rings of the adenine moiety find enough space in the upper part of the active-site pocket (Fig. 6). The flexible panthothenate unit, with a stretched out dimension of about 20 Å, extends down the active site in order to react with Glu54B. The reaction with Glu54B is facilitated by the activation through hydrogen bonds to Gln103A and Gly137B. In the later steps (b and c of Fig. 1) of the proceeding reaction these two amide groups will form an oxyanion hole, thereby stabilizing the evolving negative charge on the Glu54B carbonyl oxygen of the tetrahedral transition state. In steps (a) and (d) of Figure 1 an oxyanion is generated on the carbonyl oxygen

Figure 6

The active-site residues of subunit B. Stereo diagram of the active site, as seen from subunit A, showing the clustering of conserved residues (green) from subunit B lining the active site. Glu54B is located at the bottom of the figure and the active-site funnel opens to the top. Lys10B and Arg157B, which are proposed to participate in CoA-binding are labelled. Gln103A and Gly137B, which are involved in hydrogen bonding (thin white lines) to Glu54B are also labelled. The model is covered by $2F_o–F_c$ electron density contoured at 1σ. A model of coenzyme A (white) in a hypothetical conformation is included in the figure. (The figure was produced using MAIN [45].)

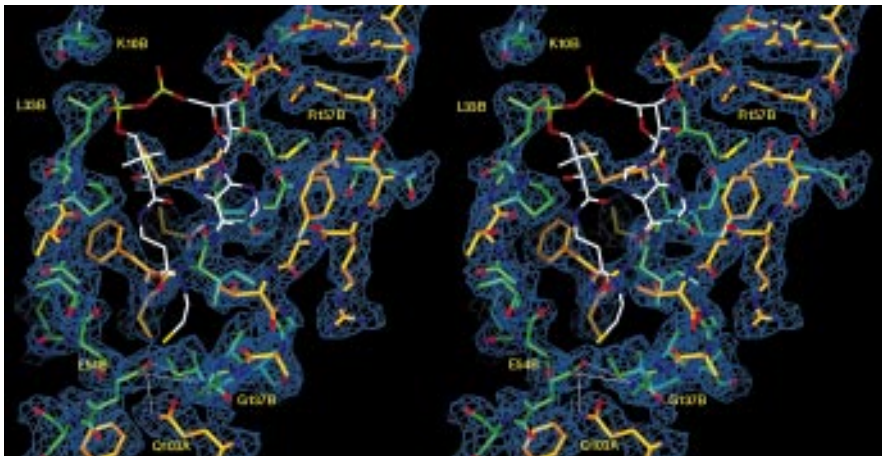

Figure 7

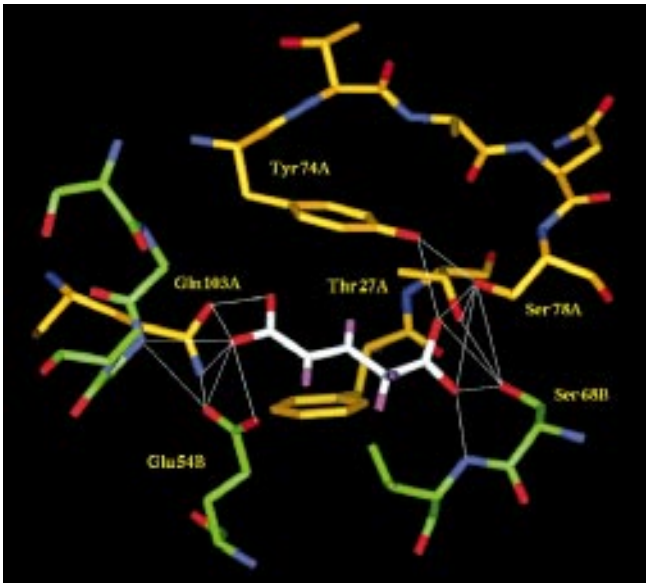

The proposed substrate-binding pocket of GCT. Close-up of the proposed substrate-binding pocket. A modelled glutaconate molecule (white) is involved in numerous hydrogen bonds (thin white lines) to residues of GCT subunit A (yellow) and subunit B (green).

of the substrates R1 and R2. Possible candidates for stabilization are the amide nitrogens of Ala138B and Gly137B. The substrate specificity towards five carbon atom containing dicarboxylic acids may be explained by the presence of the two serine residues Ser78A and Ser68B. These residues are located in a small side pocket of the active site with both of their sidechain oxygens at a distance of 9.0 Å from the active-site residue Glu54B, which corresponds to the expected length of a substrate in an extended conformation. The orientation of these serine residues enables them to be involved in simultaneous hydrogen bonding to both carbonyl oxygens of the γ-carboxyl group of the substrate (Fig. 7).

Comparison with related enzymes

An alignment of the known amino acid sequences of CoA-transferases is shown in Figure 8. It is well known that despite low sequence similarity some proteins adopt similar folds. Both subunits of GCT share low sequence similarity with other CoA-transferases and almost no similarity to each other, whereas the sequences of the other CoA-transferases exhibit strong sequence correlation within related subunits. An alignment based on the amino acid sequence could not establish an obvious relation between GCT and the other CoA-transferases. However, within the course of refinement it was found that large parts of both GCT subunits are spatially superimposable. The structural similarity covers the N-terminal region from the N terminus to strand β10 in subunit A and its counterpart β9 in subunit B. This structural alignment

Figure 8 legend

Alignment of the sequences from known CoA-transferases. The upper part of the figure shows a structure-based alignment of both subunits of *A. fermentans* GCT as calculated with the program GBF-3D-fit [41]. The upper and lower rows of numbering refer to the sequences of GCT subunits A and B, respectively. Similar residues are typed in bold face and residues with a Cα distance of less than 3 Å in the superimposed models are coloured orange. The residues 57B–59B of subunit B align out of sequence, as the direction of strand β3 is reversed. The secondary structure elements are also indicated and labelled according to Figure 2. The lower part of the figure shows the alignment of the amino acid sequences from other CoA-transferases to the profile given in the upper part using routines from the GCG package [42]. Similar residues in subunit A chains of CoA-transferases are coloured blue and those in B chains are in yellow; residues that are conserved within both types of chains are typed in red. Arrows point to conserved residues that are in contact with the active site (the catalytic residue, Glu54B, is marked by a green arrow). The mitochondrial leader sequence of the pig heart CoA-transferase is typed in green. The sequences of CoA-transferases from five different organisms were used in the alignment: Afe, GCT from *A. fermentans*; Aca, 3-oxoadipate-CoA-transferase from *Acinetobacter calcoaceticus*; Ppu, 3-oxoadipate-CoA-transferase from *Pseudomonas putida*; pig, 3-oxoacid-CoA-transferase from pig heart mitochondria; Cac, butyrate acetoacetate-CoA-transferase from *Clostridium acetobutylicum*. (The figure was produced with the program ALSCRIPT [46].)

suggested that both subunits may have evolved from a common ancestor which adapted to the different purposes of catalysis and oligomerization.

A consensus matrix was derived from this structural alignment and used in a database search for related sequences. The four highest similarity scores were obtained for three CoA-transferase chains (two from subunit B, one from subunit A) and a hypothetical protein from the influenza virus. The known amino acid sequences of all CoA-transferases, including those with lower similarity scores, were aligned against the structural alignment of the GCT subunits A and B. For this purpose the amino acid sequence of the homodimeric pig heart 3-oxoacid CoA-transferase was aligned in two pieces, as the N-terminal part of the pig heart enzyme corresponds to the sequences of the bacterial A subunits and the C-terminal part to those of bacterial B subunits [12]. The proposed gene fusion that has linked the bacterial A and B subunits could have occurred in a subunit arrangement as found in GCT, as the C terminus of subunit A is in close spatial proximity to the N terminus of subunit B, as can be seen in Figure 3.

The lower part of Figure 8 shows the complete alignment of CoA-transferase amino acid sequences with the consensus sequence derived from the structural alignment of GCT subunits A and B. The sequence similarity for subunit B is not significant (20%); only some stretches of similarity are found in subunit A.

Amino acid residues that contribute to the active site are frequently conserved, especially in subunit B. All other CoA-transferase sequences that align with the sequences

Figure 8

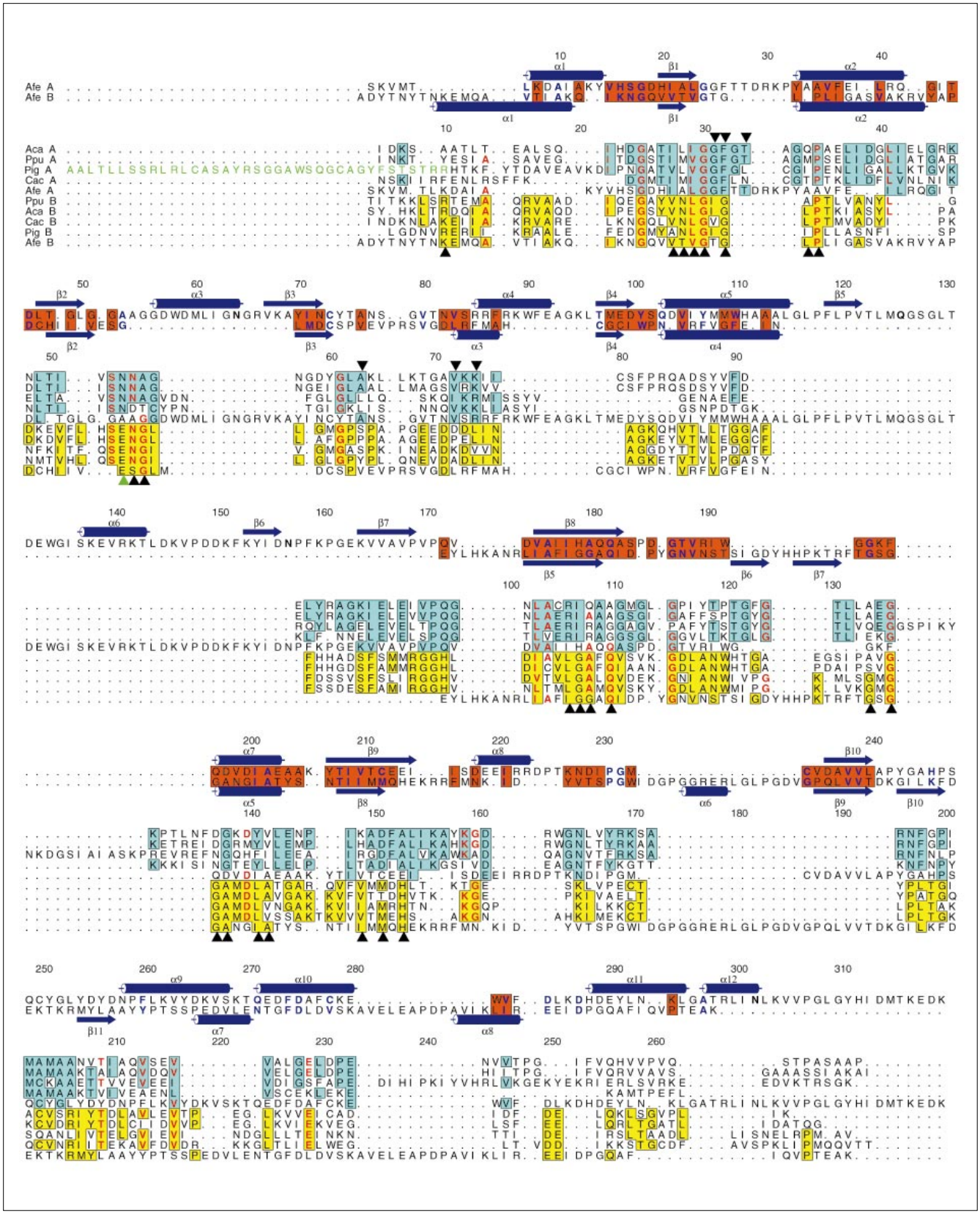

of the GCT subunits are compatible with the secondary structure so that neither proposed helices nor strands are disrupted. Structurally important glycine and proline residues tend to be conserved. All other CoA-transferases resemble the tetrameric state of oligomerization, but none of them can be regarded as an octamer. Consequently, none of the sequences are homologous to the C-terminal region of subunit A responsible for octamer formation.

In summary, it can be predicted that all CoA-transferases belong to the open α/β-protein class with an overall topology comparable to GCT and that they have a similar position and architecture of the active sites.

Biological implications

Coenzyme A esters are biologically important compounds, especially in the metabolism of amino acids and lipids. Among the various enzymatic ways to form these acyl-CoA derivatives, the transfer of the CoA moiety from an already existing CoA ester to a carboxylate is the most economic way. CoA-transferases are abundant in anaerobic fermenting bacteria which have to cope with low ATP yields, but they are also found in aerobic bacteria and in the mitochondria of humans and other mammals. The human succinyl-CoA:3-oxoacid CoA-transferase (SCOT) catalyzes the rate-limiting step in the utilization of ketone bodies. SCOT deficiency is a metabolic disease, which manifests itself in episodes of severe ketoacidosis. CoA-transferases are diverse in substrate specificity as well as subunit composition, ranging from monomers (A) to heterooctamers $(AB)_4$. Nevertheless, all of them follow a similar reaction mechanism.

We have solved the structure of the glutaconate CoA-transferase (GCT) from the anaerobic bacterium *Acidaminococcus fermentans*. GCT is a heterooctamer $(AB)_4$, $M_w = 260$ kDa, which catalyzes the reversible transfer of the CoA moiety from acetyl CoA to (*R*)-2-hydroxyglutarate and related compounds in the fermentation pathway of glutamate. This reaction proceeds, as within other CoA-transferases, via a ping-pong mechanism, where a covalent intermediate exists with the CoA bound as part of a thiol ester to the active-site residue. Labelling and mutational studies proved that the active-site residue is Glu54 on subunit B (Glu54B) of GCT. The catalytic unit of GCT is the AB heterodimer, so that the whole enzyme carries four active sites located at the interfaces of subunits A and B. The funnel-shaped opening to the active site has a depth and diameter of about 20 Å with the catalytic residue Glu54B located at the bottom. Glu54B is hydrogen bonded to four close amide protons, that will therefore be involved in stabilizing the tetrahedral transition state in the catalytic reaction. Both subunits of GCT, A and B, belong to the open **α/β**-protein class and reveal spatial similarity, despite lacking amino acid sequence similarity. With these findings it could be shown that GCT is homologous to other CoA-transferases. Therefore, a similar overall fold and a comparable position and architecture of the active site for all CoA-transferases can be proposed.

This structure of GCT provides the basis for further studies with CoA ester and carboxylate complexes in combination with specific mutants of GCT. With such studies the hypotheses from this paper, regarding the role of the amides stabilizing the active-site glutamate and the mode of substrate binding, could be tested. Furthermore, these studies might help to explain kinetic data, which showed a conversion of binding energy between enzyme and substrate into rate enhancement of the overall reaction.

Materials and methods

Purification

Glutaconate coenzyme A-transferase (GCT) from *A. fermentans* was expressed in *E. coli* and purified as described by Mack *et al.* [3]. During this procedure the protein was precipitated with ammonium sulphate in a microcrystalline form in which it was stable for several months.

Crystallization

The microcrystals were dissolved (20 mg ml^{-1} protein, 750 mM ammonium sulphate, 5 mM Mes pH 5.5) and 4 μl of this solution were mixed with 1 μl from the reservoir solution (1.65 M ammonium sulphate, 0.1 M Mes pH 5.5, 1 mM $CuSO_4$, 5% PEG 8000). This mixture was equilibrated against 1 ml of the reservoir solution at 20°C in Chryschem plates (Charles Supper) using the sitting-drop vapour diffusion method. Orthorhombic crystals (space group $C222_1$ of cell dimension a = 145.12 Å, b = 152.27 Å, c = 130.61 Å) which contained half of the octamer in the asymmetric unit appeared in three to four days. Within two weeks the crystals reached their final size of approximately $100 \times 120 \times 500$ mm and were harvested in the reservoir solution with an increased ammonium sulphate concentration (1.9 M) but without $CuSO_4$.

Preparation of heavy-atom derivatives

The heavy-atom derivatives were prepared by soaking crystals in the harvesting solution to which the heavy-metal component in question had been added (Table 2).

X-ray data collection and processing

Diffraction data from native and heavy-atom derivatized crystals were collected on an image plate system (MAR research) using graphite monochromatized CuK_α radiation from a RU200b rotating-anode generator (Rigaku) operated at 45 kV and 120 mA. The reflections were integrated with the program MOSFLM [33] and subsequently the data was scaled, reduced and truncated to obtain the structure-factor amplitudes using routines from the CCP4 program suite [31].

Structure determination

The structure was solved with the standard procedures of the MIR method. From the large number of soaks carried out with different heavy-atom components only the organic mercury compounds thiomersalate (THM) and 2-mercury-4-diazo-benzoic-acid (MQB) gave interpretable difference Patterson maps. The major heavy-atom positions for each derivative were determined from difference Patterson maps and initial phases were calculated. These positions were confirmed, minor sites and a weaker rhenium derivative were added employing cross-difference Fourier maps using the program PROTEIN [34]. The heavy-atom parameters were further refined with the program MLPHARE [31] leading to the statistics shown in Table 2. An electron-density map was calculated and the phases were improved further by solvent flattening, histogram matching and application of Sayre's equation with the

Table 2

Data collection and phasing statistics.

Compound	Resolution (Å)	Completeness (%)	Multiplicity	R merge* (%)	Concentration (mM)	Time of soak (days)	R_{iso}†	No. of sites (sites)	Phasing‡ power		R_{cullis}§	
									cent.	acent.	cent.	acent.
Native	2.5	83.6	2.8	9.8								
THM	3.5	84.7	3.4	6.9	10	0.5	28.9	4 (A,B,C,D)	1.02	1.61	0.79	0.73
MQB	3.0	97.6	3.8	5.4	saturated	0.5	26.0	4 (B,C,D,E)	1.10	1.58	0.76	0.72
CTM1	3.3	69.1	3.4	5.8	††	0.5	25.9	1 (D)	0.90	1.43	0.80	0.73
CTM2	3.5	73.8	3.5	6.7	††	1.0	29.4	2 (C,D)	0.91	1.40	0.80	0.74
K_2RhCl_6	3.5	93.9	3.6	6.0	4	0.5	18.8	1(F)	0.43	0.63	0.92	0.93

*$R_{merge} = \Sigma | I_{obs} - < I > | / \Sigma I_{obs}$; †$R_{iso} = \Sigma | F_{der} - F_{nat} | / \Sigma F_{nat}$, where the summation is over all reflections. ‡Phasing power = F_h/A, where F_h is the heavy-atom structure-factor amplitude and A the residual lack of closure; §R_{cullis} = lack of closure / isomorphous difference. The abbreviations used are: THM, thiomersalate; MQB, 2-mercury-4-diazo-benzoic acid; CTM, soak of THM and MQB together. ††Thiomersal (5 mM) + saturated MQB. The overall figure of merit was 0.62.

program DM [31]. It can be seen from the distribution of heavy-atom sites that the four mercury derivatives are not completely independent, and the resulting electron-density map calculated to 3.0 Å was not interpretable unless it was averaged across the ncs operator.

GCT is an $(AB)_4$ octamer in solution [35], but it was estimated from the solvent content of the crystals that the asymmetric unit contains an $(AB)_2$ tetramer [36]. If the GCT tetramer obeys 222 symmetry, as tetramers frequently do, the local twofold axis must intersect one of the crystallographic dyads at an angle of 90°. Calculating a self-rotation function with the program GLRF [37] in the resolution range 8–4 Å revealed the orientation of the local axis. As the heavy-atom positions were not related by this local twofold axis a one-dimensional real space translation search along the crystallographic twofold axis in the MIR density was performed with the program PROTEIN [34]. After averaging the electron density with the program AVE [38] the core of the structure was easily built into the electron-density map. Model building was performed using the program 'O' [39] and the model was refined using the program X-PLOR [40]. The remaining parts of the molecule were built in several iterative steps of refinement, phase combination, averaging and manual adjustment of the model. All new parts of the model were built identically in the two ncs related views of the model. After model building was completed both ncs related views were manually and independently adjusted and the model was refined against the native data set merged from two crystals at the full resolution of 2.5 Å (Table 1), without ncs restrains. This model was subjected to a restrained B-factor refinement, resulting in an rms deviation of bonded B factors of 2.8 $Å^2$. Water molecules were built if the corresponding difference electron-density map was at least 3σ and geometric requirements for hydrogen bonding were fulfiled. These waters were accepted if they retained a B factor of less than 80 $Å^2$ in the following refinement.

Amino acid sequence alignment

During structure analysis it was found that the spatial structure of subunit A could be partially superimposed with subunit B. A structural alignment was carried out using the program GBF-3dfit [41]. The result was translated into a consensus sequence and subsequently used in a data bank search. This and the resulting sequence alignment were carried out using routines from the GCG package [42].

Accession numbers

The coordinates for GCT have been deposited in the Protein Data Bank, with accession code 1poi.

Acknowledgements

We thank S Liemann for helpful discussions and L Prade for preparing the 2-mercury-4-azido-benzoic acid compound. The work was supported by the Behringwerke AG, Marburg, Germany.

References

1. Lynen, F., Reichert, E. & Rueff, L. (1951). Zum biologischen Abbau der Essigsäure VI. 'Aktivierte Essigsäure', ihre Isolation aus Hefe und ihre chemische. *Natur Justus Liebigs Ann. Chem.* 574, 1–32.
2. Buckel, W., Dorn, U. & Semmler, R. (1981). Glutaconate CoA-transferase from *Acidaminococcus fermentans*. *Eur. J. Biochem.* 118, 315–321.
3. Mack, M., Bendrat, K., Zelder, O., Eckel, E., Linder, D. & Buckel, W. (1994). Location of the two genes encoding glutaconate coenzyme A-transferase at the beginning of the hydroxyglutarate operon in *Acidaminococcus fermentans*. *Eur. J. Biochem.* 226, 41–51.
4. Tung, K.K. & Wood, W.A. (1975). Purification, new assay, and properties of coenzyme A transferase from *Peptostreptococcus elsdenii*. *J. Bacteriol.* 124, 1462–1474.
5. Sramek, S.J. & Frerman, F.E. (1975). Purification and properties of *Escherichia coli* coenzyme A-transferase. *Arch. Biochem. Biophys.* 171, 14–26.
6. Barker, H.A., Jeng, I.M., Neff, N., Robertson, J.M., Tam, F.K. & Hosaka, S. (1978). Butyryl-CoA: acetoacetate CoA-transferase from a lysine-fermenting *Clostridium*. *J. Biol. Chem.* 253, 1219–1225.
7. Schweiger, G. & Buckel, W. (1984). On the dehydration of (*R*)-lactate in the fermentation of alanine to propionate by *Clostridium propionicum*. *FEBS Lett.* 171, 79–84.
8. Wiesenborn, D.P., Rudolph, F.B. & Papoutsakis, E.T. (1989). Coenzyme A-transferase from *Clostridium acetobutylicum* ATCC 824 and its role in the uptake of acids. *Appl. Environ. Microbiol.* 55, 323–329.
9. Eikmanns, U. & Buckel, W. (1990). Properties of 5-hydroxyvalerate CoA-transferase from *Clostridium aminovalericum*. *Biol. Chem. Hoppe Seyler* 371, 1077–1082.
10. Scherf, U. & Buckel, W. (1991). Purification and properties of 4-hydroxybutyrate coenzyme A transferase from *Clostridium aminobutyricum*. *Appl. Environ. Microbiol.* 57, 2699–2702.
11. Baetz, A.L. & Allison, M.J. (1990). Purification and characterization of formyl coenzyme A-transferase from *Oxalobacter formigenes*. *J. Bacteriol.* 172, 3537–3540.
12. Parales, R.E. & Harwood, C.S. (1992). Characterization of the genes encoding beta ketoadipate succinyl-coenzyme A-transferase in *Pseudomonas putida*. *J. Bacteriol.* 174, 4657–4666.
13. White, H. & Jencks, W.P. (1976). Properties of succinyl-CoA: 3-ketoacid coenzyme A transferase. *J. Biol. Chem.* 251, 1708–1711.
14. Sharp, J.A. & Edwards, M.R. (1978). Purification and properties of succinyl-coenzyme A-3-oxo acid coenzyme A-transferase from sheep kidney. *Biochem. J.* 173, 759–765.
15. Russel, J.J. & Patel, M.S. (1982). Purification and properties of succinyl-CoA: 3-oxo-acid CoA-transferase from rat brain. *J. Neurochem.* 38, 1446–1452.
16. Blair, J. (1969). Skeletal muscle coenzyme A transferase. *J. Biol. Chem.* 244, 951–954.
17. Lin, T. & Bridger, W.A. (1992). Sequence of a cDNA clone encoding pig heart mitochondrial CoA-transferase. *J. Biol. Chem.* 267, 975–978.
18. Gerischer, U. & Dürre, P. (1990). Cloning, sequencing, and molecular analysis of the acetoacetate decarboxylase gene region from *Clostridium acetobutylicum*. *J. Bacteriol.* 172, 6907–6918.

19. Buckel, W. (1976). Acetic anhydride: an intermediate analogue in the acyl-exchange reaction of citramalate lyase. *Eur. J. Biochem.* 64, 263–267.
20. Buckel, W. & Bobi, A. (1976). The enzyme complex citramalate lyase from *Clostridium tetanomorphum*. *Eur. J. Biochem.* 64, 255–262.
21. Dimroth, P. & Eggerer, H. (1976). Isolation of subunits of citrate lyase and characterization of their function in the enzyme complex. *Proc. Natl. Acad. Sci. USA* 72, 3458–3462.
22. Dimroth, P., Buckel, W., Loyal, R. & Eggers, H. (1977). Characterization of the subunits of citramalate lyase and their function in the enzyme complex. *Eur. J. Biochem.* 80, 469–477.
23. Jencks, W.P. (1973). Coenzyme A transferases. In *The Enzymes*. (Boyer, P.D., ed.), pp. 483–496, Academic Press, New York.
24. Schweiger, G., Dutscho, R. & Buckel, W. (1987). Purification of 2-hydroxyglutaryl-CoA dehydratase from *Acidaminococcus fermentans*: an iron–sulfur protein. *Eur. J. Biochem.* 169, 441–448.
25. Mack, M. & Buckel, W. (1995). Identification of glutamate beta-54 as the covalent-catalytic residue in the active site of glutaconate CoA-transferase from *Acidaminococcus fermentans*. *FEBS Lett.* 357, 145–148.
26. Luzzati, P.V. (1952). Traitement statistique des erreurs dans la détermination des structures cristallines. *Acta Cryst.* 5, 802–810.
27. Engh, R.A. & Huber, R. (1991). Accurate bond and angle parameters for X-ray protein structure refinement. *Acta Cryst.* 47, 392–400.
28. Kleywegt, G.J. & Jones, T.A. (1994). A super position. *EFS/CCP4 Newsletter* 31, 9–14.
29. Ramachandran, G.N. & Sasisekharan, V. (1968). Conformation of polypeptides and proteins. *Adv. Protein Chem.* 23, 283–437.
30. Richardson, J.S. (1981). Protein Anatomy. *Adv. Protein Chem.* 34, 167–339.
31. Collaborative Computational Project No.4. (1994). The CCP4 suite: programs for protein crystallography. *Acta Cryst. D* 50, 760–763.
32. Branden, C. & Tooze, J. (1991). Introduction to Protein Structure. Garland Publishing, London.
33. Leslie, A.G.W. (1994). *Mosflm User Guide: Mosflm Version 5.20*. MRC Laboratory of Molecular Biology, Cambridge, UK.
34. Steigemann, W. (1974). *Die Entwicklung und Anwendung von Rechenverfahren und Rechenprogrammen zur Strukturanalyse von Proteinen*. PhD thesis, Technische Universität München, FRG.
35. Buckel, W. & Barker, H.A. (1974). Two pathways of glutamate fermentation. *J. Bacteriol.* 117, 1248–1260.
36. Matthews, B.W. (1978). X-ray structure of proteins. In *The Proteins III*. (Neurath, H. & Hill, P.C., eds), pp. 403–590, Academic Press, New York.
37. Tong, L. & Rossmann, M.G. (1990). The locked rotation function. *Acta Cryst.* 46, 783–792.
38. Kleywegt, G.J. & Jones, T.A. (1993). Masks made easy. *ESF/CCP4 Newsletter* 28, 56–59.
39. Jones, T.A., Zou, J.Y. & Kjeelgaard, M. (1991). Improved methods for building protein models in electron-density maps and location of errors in these models. *Acta Cryst. A* 47, 110–119.
40. Brünger, A.T. (1992). *X-PLOR Version 3.1. A System for X-ray Crystallography and NMR*. Yale University Press, New Haven, CT.
41. Lessel, U. & Schomburg, D. (1994). Similarities between protein 3-D structures. *Protein Eng.* 7, 1175–1187.
42. Genetics Computer Group. (1994). Program Manual for the Wisconsin Package Version 8. Madison, Wisconsin.
43. Kraulis, P.J. (1991). MOLSCRIPT: a program to produce both detailed and schematic plots of protein structures. *J. Appl. Cryst.* 24, 946–950.
44. Nicholls, A., Sharp, K.A. & Honig, B. (1991). Protein folding and association: insights from the interfacial and thermodynamic properties of hydrocarbons. *Proteins* 11, 281–296.
45. Turk, D. (1988). Development and usage of a molecular graphics program. PhD thesis, University in Ljubljana, Slovenia.
46. Barton, G.C. (1993). ALSCRIPT: tool to format multiple sequence alignments. *Protein Eng.* 6, 37–40.